Hindawi
Mathematical Problems in Engineering
Volume 2022, Article ID 5943376, 14 pages
https://doi.org/10.1155/2022/5943376

*Research Article*

# Rössler-like Neuronal Firing with Local Amplitude Control

**Zhinan Li,[1,2] Chunbiao Li,[1,2] Akif Akgul,[3] Lvqing Bi,[4] and Yicheng Jiang[1,2]**

[1]*Jiangsu Collaborative Innovation Center of Atmospheric Environment and Equipment Technology (CICAEET), Nanjing University of Information Science & Technology, Nanjing 210044, China*
[2]*School of Artificial Intelligence, Nanjing University of Information Science & Technology, Nanjing 210044, China*
[3]*Department of Computer Engineering, Faculty of Engineering, Hitit University, Corum 19030, Turkey*
[4]*School of Physics and Telecommunications Engineering, Yulin Normal University, Yulin 537000, Guangxi, China*

Correspondence should be addressed to Akif Akgul; akifakgul@hitit.edu.tr

Received 20 October 2022; Revised 30 November 2022; Accepted 2 December 2022; Published 15 December 2022

Academic Editor: Zenghui Wang



Chaotic neuronal oscillation is fired up when a locally active memristor is introduced into the Rössler system. Such a memristive Rössler system has two independent parameters providing local amplitude control, one of which even adjusts the amplitude and frequency of variables in a specific intermittent mode. Different neuronal firing modes are modified by the system parameter. The coexistence of periodic oscillation and chaos is also captured along with basin of attraction. STM32-based experiment verified the numerical and theoretical results.

## 1. Introduction

In 1971, Chua predicted that the memristor is the fourth basic component of the circuit [1–7]. Memristor can be regarded as a perfect device to simulate synapses because of its memory effect and nonlinearity. In 2008, Hewlett–Packard laboratory proposed a $TiO_2$ memristor and claimed that the memristor cross-switch matrix is the only technology with the ability to mimic human neurons [8]. The research on memristor has been rapidly carried out in the industrial field and academia. Many theoretical models and circuit models of memristors have been developed [9–12]. Many scholars introduced memristor into the system and constructed great number of chaotic systems for engineering application [13–21].

In recent years, the research on locally active memristor has aroused people's interest. Compared with the general memristor, the emergence of locally active memristors makes the neuromorphic dynamics behavior possible [22–24]. Considering many memristors such as the Chua's Corsage Memristor (CCM) [25] and those chaotic systems with offset boosting and amplitude control [26–28], memristor does bring great new dynamics to the existing systems. Jin et al. [29] proposed an extended chaotic circuit based on CCM and analyzed its neuromorphic dynamical behavior. Lin et al. [30] investigated a new locally active memristor model and applied it to the HR neuron, and multistability with coexisting firing patterns were discussed. Two fractional-order memristive HR neurons are coupled together [31], and hyperchaotic attractors and hidden coexisting oscillations can be found. A simple locally active memristor was introduced into the HR neurons [32], and coexisting attractors were found. Memristor was added in the Hopfield neural network for producing multi-double-scroll attractors [33], where coexisting attractors caused by the initial offset boosting were proposed. The oscillation in the Rössler system is unique and has attracted some attention in nonlinear community. In 2017, a memristive function is inserted into the Rössler system for obtaining initial-dependent coexisting dynamics, and the role of the initial memristive variable for synchronization stability is discussed [34].

In this work, a locally active memristor is introduced into the Rössler system. Locally active memristor brings some new features into the revised Rössler system. It is found that the oscillator has unique properties, including local

amplitude control, local amplitude/frequency control, neuromorphic behavior of bursting, and coexisting attractors. The properties of the new oscillator are shown in Figure 1.

Compared with other memristive chaotic systems, the newly constructed oscillator has the following properties:

(1) There are two independent local amplitude controllers, one of which adjusts the amplitude and frequency of variables while the other rescales system variable under a unified set of Lyapunov exponents.

(2) Many dynamics are inherited in the memristive Rössler system even when a locally active memristor is introduced. But further observation shows that neuronal oscillation is fired up.

(3) Coexisting neuromorphic firing including the coexistence of a limit cycle and chaotic attractor is found. Basins of attraction are given.

A comparison with existing memristive neuron systems is listed in Table 1. The evaluation focusing on three aspects includes locally active memristor included (LAM), local amplitude control (LAC), and local frequency control (LFC). LAC and LFC represent the stability of a parameter, which prefers modifying the signal features rather than bring unpredicted bifurcation.

The following of this report is organized as follows: In Section 2, a locally active memristor is introduced in the Rössler system, where basic analysis of the memristor is given. In Section 3, dynamic behavior of the new proposed Rössler-like memristive system is analyzed based on the bifurcation. In Section 4, the discharge behavior and coexisting attractors are demonstrated. In Section 5, STM32-based verification is given. The conclusion is rapped in the last section.

## 2. A Memristive Rössler System with a Locally Active Memristor

*2.1. Model Description and Chaotic Firing.* Inspired by the works [25, 29, 35], the locally active memristor is introduced into the Rössler system, and a new four-dimensional chaotic system is constructed as follows:

$$\begin{cases} \dot{x} = -y - w^2 z, \\ \dot{y} = x + ay, \\ \dot{z} = b + z(x - c), \\ \dot{w} = 0.2(30 - w + |w - 20| - |w - 40|) + z. \end{cases} \tag{1}$$

Here, CCM is introduced into the first dimension, whose internal variable obeys the constriction from the fourth dimension. When $a = 0.4$, $b = 0.05$, $c = 20$ and initial conditions (IC) (−9, 0, 0, −1), system (1) exhibits chaotic oscillation, as shown in Figure 2. The attractor has Lyapunov Exponents (LEs) of (0.1650, 0, −0.2187, −15.5081) and the Kaplan–York dimension of 2.7543. The waveforms diagram is shown in Figure 3.

While $w > 40$, $a = 0.4$, $b = 0.001$, $c = 20$ and IC = (−9, 0, 0, 50), system (1) exhibits chaos, the equilibrium points are saddle-focus, corresponding eigenvalues are listed in Table 2. When $20 < w \leq 40$, we have not found chaos in the system. Therefore, in the following, the case of $w \leq 20$ is discussed.

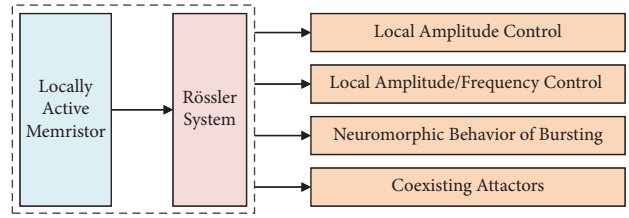


Figure 1: The properties of the new Rössler-like oscillator.

Table 1: Comparison of Rössler-like oscillator with existing memristive neurons.

| Ref | LAM | LAC | LFC |
|---|---|---|---|
| [30] | Yes | No | No |
| [32] | Yes | No | No |
| [31] | No | No | No |
| [33] | No | No | No |
| This work | Yes | Yes | Yes |

*2.2. Property of a Locally Active Memristor.* As a first-order nonvolatile locally active memristor, the mathematical expression of CCM is as follows:

$$\begin{cases} i_M = G(x)v_M = G_0 x^2 v_M, \\ \dfrac{dx}{dt} = g(x, v_M) = 30 - x + |x - 20| - |x - 40| + v_M. \end{cases} \tag{2}$$

The inductance function is represented by $G(x)$ in equation (2), where $G_0 = 1$. The current and voltage in the locally active memristor are represented by $i_M$ and $v_M$, and state variable is expressed as $x$. Inspired by the quation mentioned above, a new parameter is employed to adjust dynamical characteristics in

$$\begin{cases} i_M = G(x)v_M = G_0 x^2 v_M, \\ \dfrac{dx}{dt} = 0.2(30 - x + |x - 20| - |x - 40|) + v_M. \end{cases} \tag{3}$$

Keeping $G_0 = 1$ in equation (3), the voltage source is chosen as $V = A\sin(2\pi ft)$ to study the characteristics of the locally active memristor under various signal frequencies and amplitudes, where $A$ represents the voltage amplitude and $f$ represents the frequency. The hysteresis loop of the memory crosses the origin, as shown in Figure 4. The side lobe area increases with the increase of amplitude $A$ under $f = 0.2$. Moreover, with the increase of frequency, the side lobe area gradually decreases under $A = 0.5$. The hysteresis loop of the memristor will tend to a straight line when the frequency increases to infinity. Obviously, the constructed model accords with the basic characteristics of memristor.

The nonvolatility memory of memristors is not common to all memristors, and the power-off plot (POP) can be used

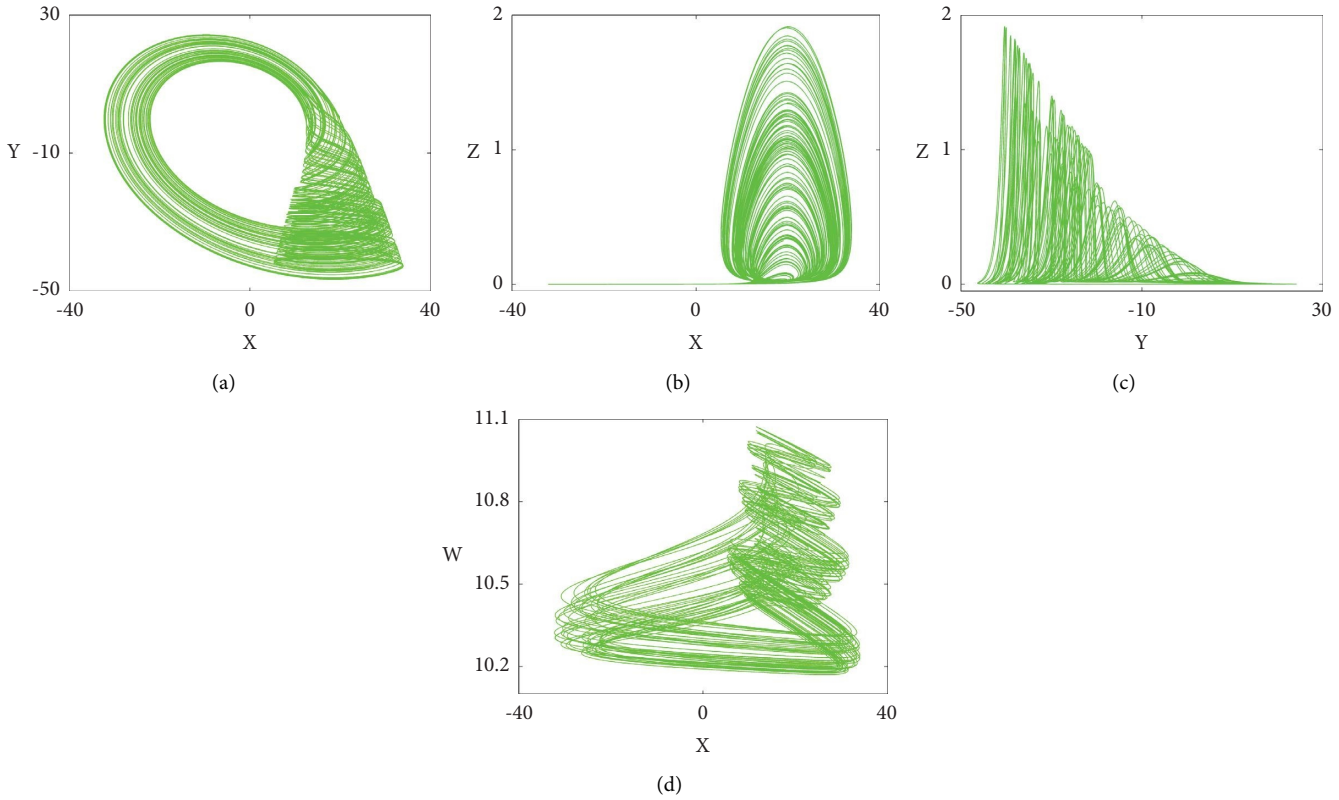


FIGURE 2: Typical chaotic phase orbits when $a = 0.4$, $b = 0.05$, and $c = 20$ under IC = (−9, 0, 0, −1) in system (1): (a) $x - y$. (b) $x - z$. (c) $y - z$. (d) $x - w$.

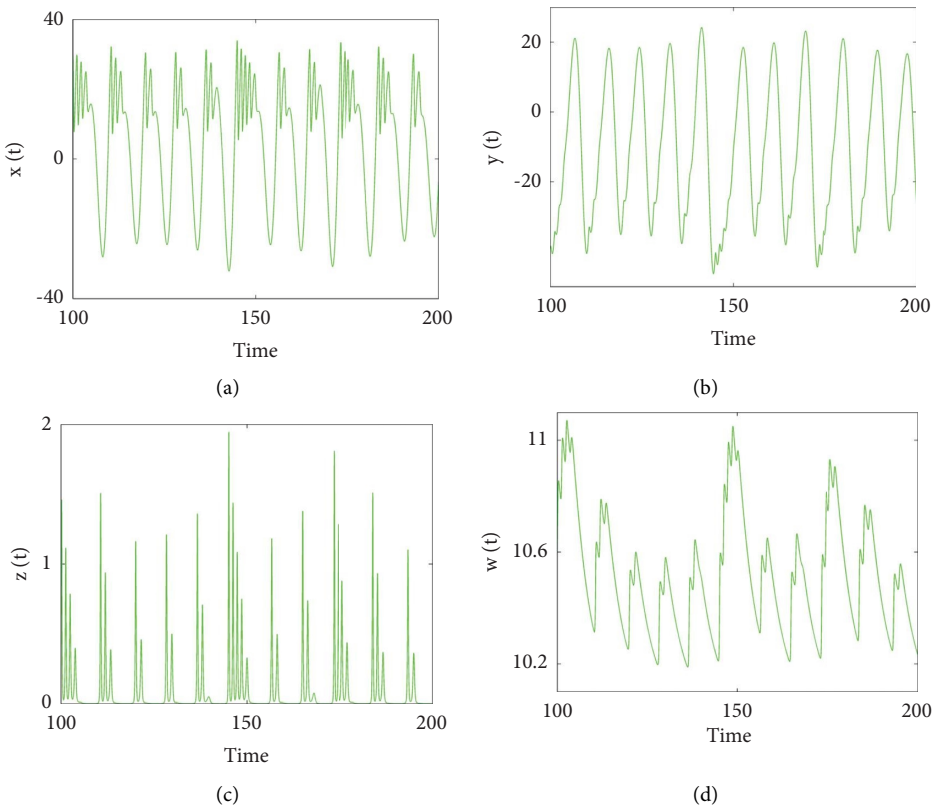


FIGURE 3: Chaotic signals of system (1) with $a = 0.4$, $b = 0.05$, and $c = 20$ under IC = (−9, 0, 0, −1): (a) $x\,(t)$. (b) $y\,(t)$. (c) $z\,(t)$. (d) $w(t)$.

Table 2: Equilibria stability of system (1) with $w > 40$, $a = 0.4$, $b = 0.001$, and $c = 20$.

| Equilibrium points | Eigenvalues | Stability |
|---|---|---|
| (19.9831, −149.8734, 0.0592, 50.2962) | −0.2023, 0.3919<br>$-0.0032 \pm 12.3641i$ | Saddle-focus of index 1 |
| (0.0167, −0.1251, 0.0001, 50.0003) | −19.9771, − 0.2000<br>$0.1969 \pm 1.7204i$ | Saddle-focus of index 2 |
| (20.0001, $-150.0007 - 0.0001i$, $-10.0296 + 0.7717i$, $-0.1482 + 3.8597i$) | −13.1745, 0.3987<br>$6.4880 \pm 2.0972i$ | Saddle-focus of index 3 |
| (20.0001, $-150.0007 + 0.0001i$, $-10.0296 - 0.7717i$, $-0.1482 - 3.8597i$) | 0.4007, 15.2005<br>$-7.7006 \pm 2.0935i$ | Saddle-focus of index 2 |

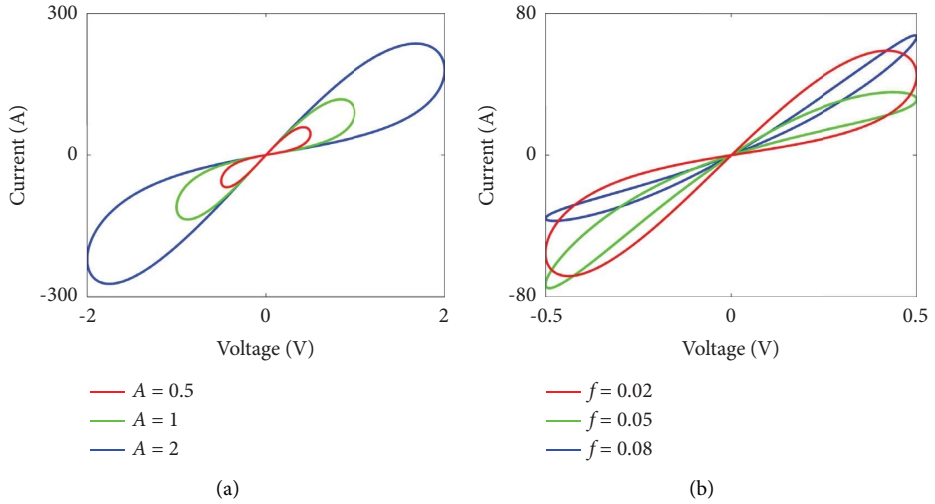


Figure 4: The hysteresis loop of the memristor $G(x)$.

to demonstrate the nonvolatility of memristors. The POP curve is a line segment with positive or negative slope in the $x - \mathrm{d}x/\mathrm{d}t$ plane when the input voltage is 0. According to the memristor nonvolatility theorem, a memristor is said to be nonvolatile when its POP curve intersects the $x$-axis with two or more negative slopes. When we let $v_M = 0$, the state equation of the memristor can be simplified to

$$\frac{\mathrm{d}x}{\mathrm{d}t} = 0.2\,(30 - x + |x - 20| - |x - 40|). \tag{4}$$

The POP curve is shown in Figure 5(a). Let $\mathrm{d}x/\mathrm{d}t = 0$, the POP curve has three intersections with the $x$-axis, which are $Q_1$ (10, 0), $Q_2$ (30, 0) and $Q_3$ (50, 0). It should be emphasized that each intersection of POP curve and $x$-axis is defined as the equilibrium point of memristor when $\mathrm{d}x/\mathrm{d}t = 0$. Therefore, there is only one stable equilibrium state for the locally active memristor under different initial states $x(0)$ as follows:

$$X = x\,(30, 0) = 30. \tag{5}$$

The local activity of the memristor can be judged by the DC $V - I$ curve. Memristor is local activity when there is a negative slope in the DC $V - I$ curve. The voltage $v_M$ can be expressed by equation (6) and the current $i_M$ can be expressed by equation (7) when $\mathrm{d}x/\mathrm{d}t = 0$.

$$v_M = -0.2\,(30 - x + |x - 20| - |x - 40|), \tag{6}$$

$$i_M = -x^2\,(0.2\,(30 - x + |x - 20| - |x - 40|)). \tag{7}$$

According to equations (6) and (7), when $x$ varies between (−10, 65), the input voltage $v_M$ takes values between (−4, 3) and the DC $V - I$ curve can be obtained, as shown in Figure 5(b). When the vertical axis current $i_M$ is 0, there are two intersections with the horizontal axis voltage $v_M$, which are (−2, 0) and (0, 0). In the red curve, there exists a curve with negative slope when the voltage takes the value of (−2, 0.668). The curves in the green and blue areas are positive. Therefore, the locally active domain of the memristor is $-2 < V < 0.668$.

*2.3. Basic Dynamical Analysis.* The dynamic evolution of system (1) can be captured by changing any parameter in the system.

*2.3.1. Equilibrium Points and Stability Analysis.* Equilibrium points can be calculated from the following equation:

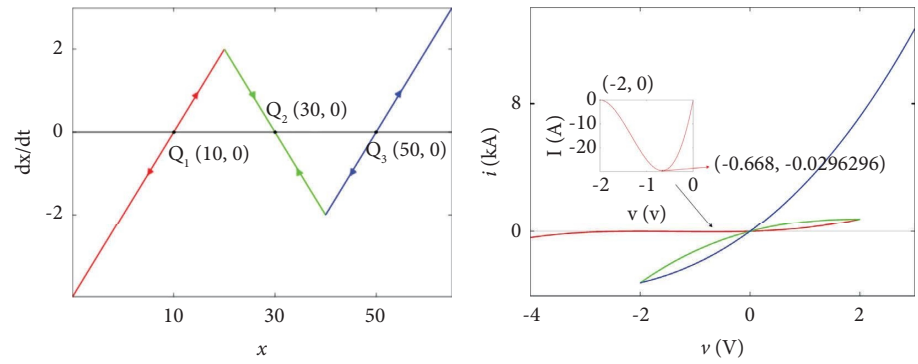


Figure 5: (a) POP curve of the memristor $G(x)$. (b) DC $V-I$ curve of the memristor $G(x)$.

$$\begin{cases} -y - w^2 z = 0, \\ x + ay = 0, \\ b + z(x - c) = 0, \\ 0.2(30 - w + |w - 20| - |w - 40|) + z = 0. \end{cases} \tag{8}$$

By calculating equation (8), a none-zero equilibrium point $S_1$ (0.1008, −0.2519, 0.0025, 10.0126) shows up in system (1). In order to calculate the eigenvalues of system (1) and understand its stability, the Jacobi matrix at this equilibrium point $S_1$ is

$$J = \begin{bmatrix} 0 & -1 & -100.2514 & -0.0503 \\ 1 & a & 0 & 0 \\ 0.0025 & 0 & 0.1008 - c & 0 \\ 0 & 0 & 1 & -0.2 \end{bmatrix}. \tag{9}$$

The characteristic equation of system (1) at this equilibrium point can be obtained as follows:

$$\begin{aligned} &\lambda^4 + (-0.1008 + c - a + 0.2)\lambda^3 - (1.2708 - 0.0992a - ac + 0.2c)\lambda^2 \\ &\quad + (0.1494 - 0.2305a - 0.2ac + c)\lambda - 0.0202 - 0.0503a + 0.2c = 0. \end{aligned} \tag{10}$$

When $a = 0.4$, $c = 20$, the equilibrium point $S_1$ is an unstable saddle-focus of index 2. The eigenvalues are $\lambda_1 = -19.8866$, $\lambda_2 = -0.1999$, $\lambda_{3,4} = 0.1936 \pm 0.9788i$.

*2.3.2. Bifurcation and Typical Solutions.* Let $a = 0.4$, $c = 20$, and IC = (−9, 0, 0, −1), when b varies in [0.05, 0.2], the corresponding Lyapunov exponents and bifurcation diagrams are plotted in Figure 6. When $b$ changes in the region of [0.05, 0.065], system (1) is in a chaotic state; when $b$ drops in [0.067, 0.0815], the system (1) orbit is periodic; when $b$ is in the range of [0.082, 0.9695], system (1) enter chaotic state; when $b$ changes in [0.105, 0.119] and [0.139, 0.153], system (1) has different chaotic attractors; as the parameter $b$ varies in [0.179, 0.2], system (1) completely enters the periodic state. Without considering each periodic window, Lyapunov exponents show a roughly linear downward trend, and the dynamical oscillation remains nearly constant in most chaotic intervals. The waveform diagrams and frequency spectrum of the signal $x(t)$ are observed when parameter $b$ is located in different intervals, as shown in Figure 7. The corresponding Lyapunov exponents and the maximum peak of the waveforms are given in Table 3.

When $a$ varies in [0.1, 0.4] with $b = 0.05$, $c = 20$ under IC = (−9, 0, 0, −1), the dynamical evolution of system (1) is shown in Figure 8. When $a$ enters in [0.1, 0.22], the periodic oscillation is given in system (1); when $a$ is in the range of [0.23, 0.283], system (1) outputs chaotic solutions; when $a$ varies in [0.284, 0.325], system (1) re-enters periodic trajectories; when $a$ increases in [0.326, 0.4], chaos emerges in system (1). Typical phase trajectories are illustrated in Figure 9, and the corresponding Lyapunov exponents are depicted in Table 4.

Set $a = 0.4$, $b = 0.05$, and the initial conditions is (−9, 0, 0, −1), the corresponding bifurcation diagrams and Lyapunov exponents when $c$ is varied in the interval of [19, 25], as shown in Figure 10. When ignoring the periodic window in the interval of [19, 25], the value of $x_m$ climbs up indicating the positively amplitude control, and the Lyapunov exponents are almost unrevised, and the dynamic behavior of the system is almost the same. Here, we call this special amplitude control as local amplitude control since it is from a bifurcation parameter rather than a nonbifurcation one. The typical phase trajectories and the waveform diagram under different $c$ shown in Figure 11 proves this finding. At the same time, in fact, the parameter $c$ also revises the amplitude of $y$, $z$, and $w$ positively [19, 25].

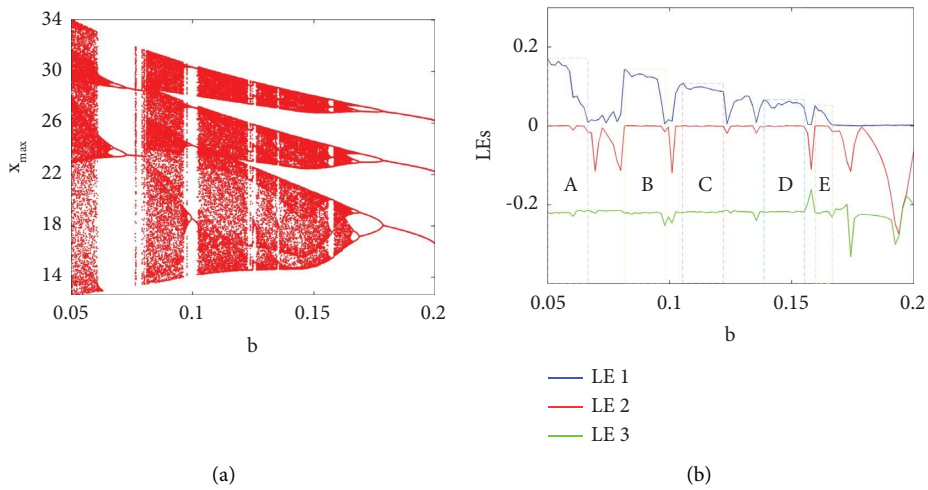


Figure 6: Bifurcation behavior of system (1) with $a = 0.4$, $c = 20$, IC $= (-9, 0, 0, -1)$, and $b$ changes in $[0.05, 0.2]$. (a) Bifurcation diagram. (b) Lyapunov exponents.

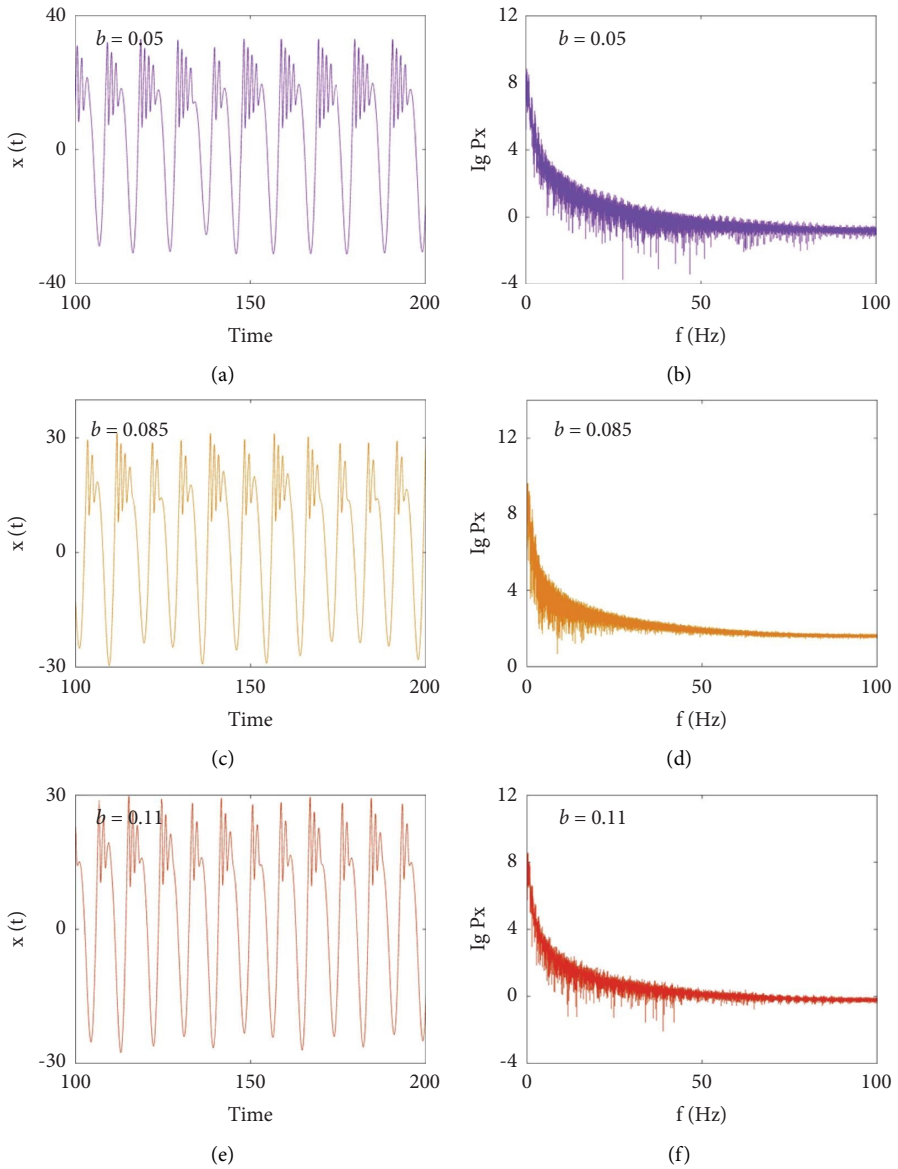


Figure 7: Continued.

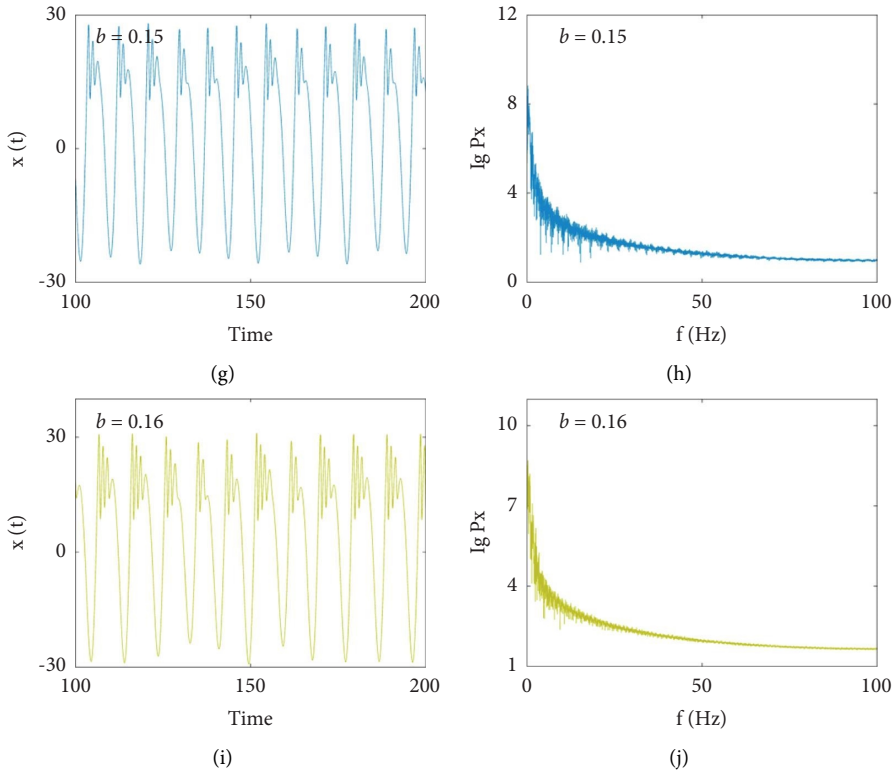


Figure 7: The waveform diagram and frequency spectrum of signal $x$ (t) under different $b$.

Table 3: Dynamical behavior of system (1) with $a = 0.4$, $c = 20$, and IC = (−9, 0, 0, −1).

| $b$ | Attractor | Lyapunov exponents | $D_{KY}$ | Maximum amplitude |
|---|---|---|---|---|
| 0.05 | Chaos | (0.1649, 0, −0.2187, −15.5081) | 2.7543 | 32.94 |
| 0.085 | Chaos | (0.1351, 0, −0.2176, −15.5551) | 2.6201 | 31.07 |
| 0.11 | Chaos | (0.1296, 0, −0.2188, −15.4828) | 2.5920 | 29.57 |
| 0.15 | Chaos | (0.0601, 0, −0.2166, −15.9513) | 2.2776 | 28.11 |
| 0.16 | Chaos | (0.0437, 0, −0.2169, −15.2015) | 2.2015 | 27.74 |

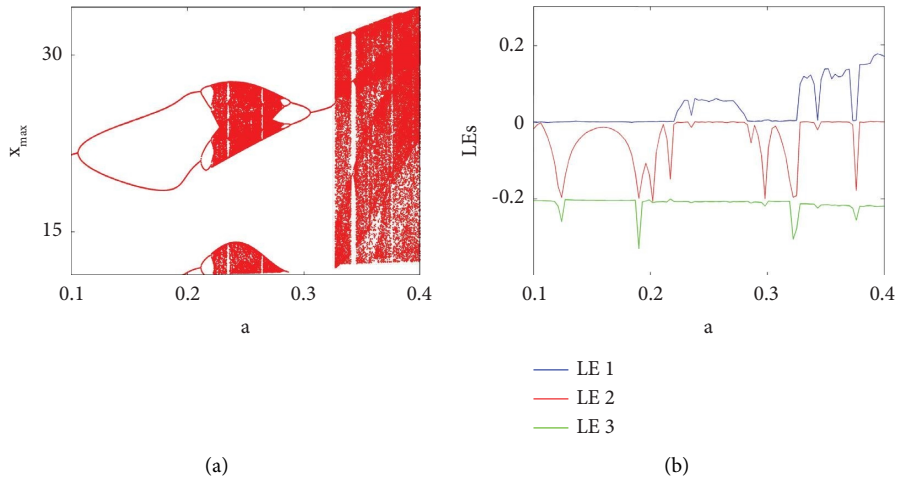


Figure 8: Dynamical evolution of system (1) with $b = 0.05$, $c = 20$, and IC = (−9, 0, 0, −1), $a$ change in [0.1, 0.4]. (a) Bifurcation diagram. (b) Lyapunov exponents.

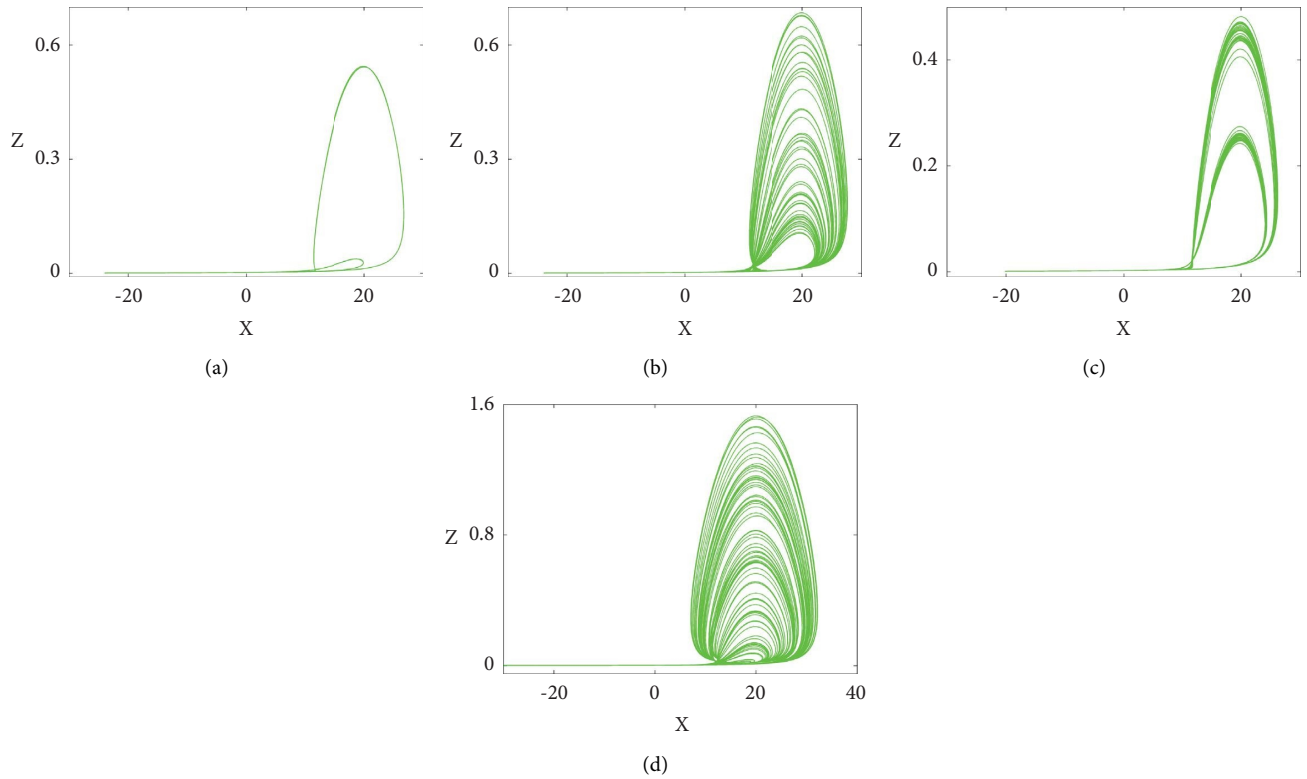


Figure 9: Typical oscillations of system (1) with $b = 0.05$, $c = 20$, and IC = (−9, 0, 0, −1). (a) $a = 0.2$. (b) $a = 0.25$. (c) $a = 0.29$. (d) $a = 0.35$.

Table 4: Dynamical behavior of system (1) with $b = 0.05$, $c = 20$, and IC = (−9, 0, 0, −1).

| $a$ | Attractor | Lyapunov exponents | $D_{KY}$ |
|---|---|---|---|
| 0.2 | Period | (0, −0.1874, −0.1874, −19.1527) | 1 |
| 0.25 | Chaos | (0.1391, 0, −0.2058, −19.0861) | 3.0003 |
| 0.29 | Period | (0, −0.0146, −0.2068, −18.7899) | 1 |
| 0.35 | Chaos | (0.1272, 0, −0.2138, −17.2382) | 2.6007 |

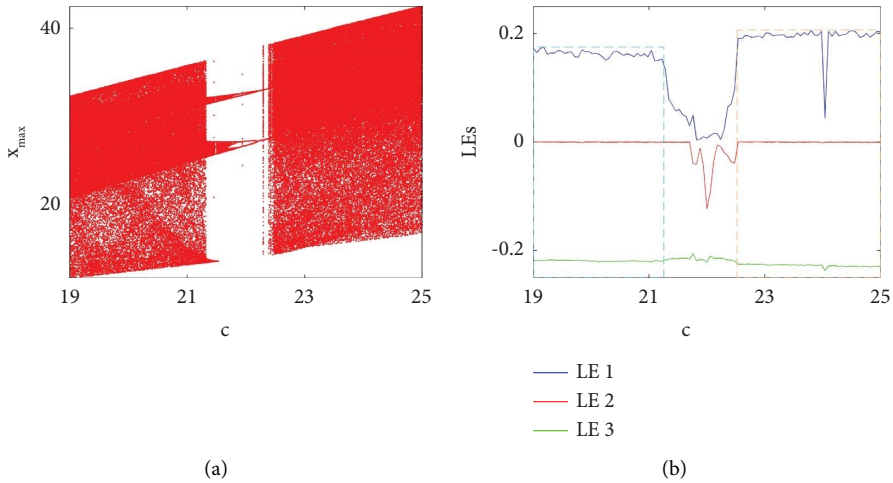


Figure 10: Bifurcation behavior of system (1) with $a = 0.4$, $b = 0.05$, and IC = (−9, 0, 0, −1), c changes in [19, 25]. (a) Bifurcation diagram. (b) Lyapunov exponents.

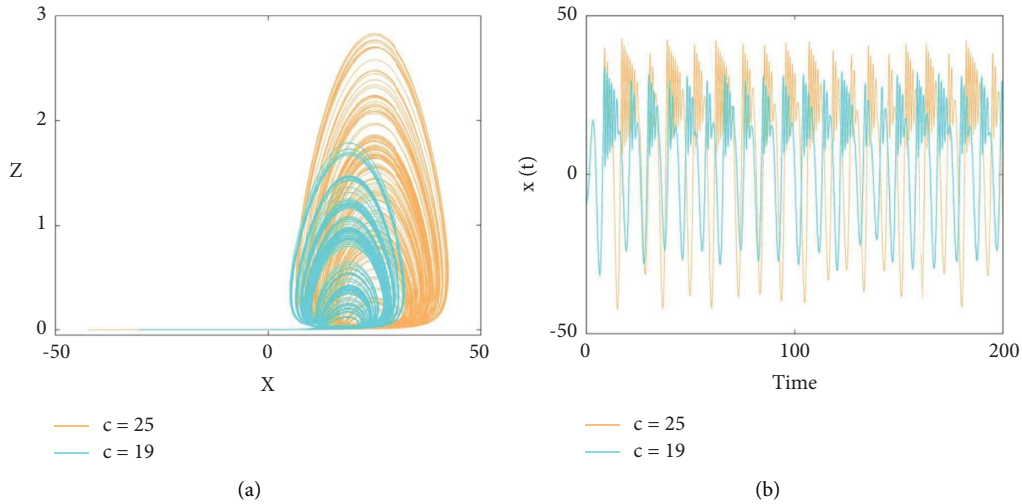


FIGURE 11: Chaotic oscillation of system (1) with $a = 0.4$, $b = 0.05$, and IC = (−9, 0, 0, −1). (a) $x - z$. (b) Chaotic signals $x(t)$. ($c = 25$ is orange, $c = 19$ is cyan.)

## 3. Neuron-like Chaotic Bursting

A unique neuromorphic firing behavior can be found after introducing a locally active memristor into the classical Rössler system. Neuronal firing patterns mainly include spiking patterns and bursting patterns [36–38]. As the name implies, spiking is a firing pattern around a signal waveform, and the bursting mainly revolves around the transformation between the stationary state of the signal and the repetitive peaks. Spiking pattern mainly includes chaotic spiking and periodic spiking. Various bursting patterns are revealed in memristive chaotic systems, which contains periodic bursting, chaotic bursting, and stochastic bursting. Periodic bursting with $n$ spikes per bursting is called periodic-$n$ bursting. In addition, the chaotic bursting includes spikes of different amplitude and number. In this work, it is found that there are chaotic bursting firing in the system and periodic bursting firing with different spikes per burst.

When we let $a = 0.4$, $c = 20$, and IC = (−9, 0, 0, −1), the neuromorphic firing behaviors of attractors in the system is explained by taking $b = 0.05$, $b = 0.1$, and $b = 0.2$. When the parameter $b$ is selected as 0.05, the chaotic bursting pattern is captured in system (1). The phase trajectories and waveform diagrams are illustrated in Figure 12. The striking phenomenon is that the peaks and period of the signal show irregular and unstable motion like the traditional neuron system.

When $b$ is fixed as 0.1, the periodic bursting pattern is depicted in Figure 13. The signals are period-3 busting firing colored in cyan. The system maintains periodic bursting pattern when $b = 0.2$, but the phase trajectories and waveform diagram of attractors change. At this time, the phase trajectories and waveform diagrams are shown in Figure 14. The signals are period-2 busting firing colored in red. In addition, the amplitude and frequency of the signals $x(t)$ and $z(t)$ when parameter $b = 0.2$ are much smaller than those when $b = 0.1$. It can be demonstrated that with the parameter $b$ is changed, the waveform diagram of the output signals $x(t)$ and $z(t)$ in the system can be transformed from chaotic bursting to periodic bursting, and the amplitude and frequency of the signals will change. The signals $x(t)$ and $z(t)$ oscillate between large amplitude and small amplitude.

## 4. Coexisting Chaotic and Periodic Bursting

Memristive chaotic systems are prone to inducing coexisting attractors due to the memory effect. Because the feedback comes from the integration process, many memristor chaotic systems have the characteristics of multistability. Coexisting attractors also exist in system (1). The coexisting attractors of the system are extracted by modifying the initial value of the system (1) when $a = 0.4$, $b = 0.1$, $c = 20$. The phase trajectories in the $x - y$ plane is depicted in Figure 15(a), where the initial conditions are (−9, 0, 0, −10) and (−9, 0, 0, −20). The Lyapunov exponents of the chaotic one are (0.0454, 0, −0.2380, −14.8243), and for the limit cycle, corresponding LEs are (0, −0.0251, −0.2321, −14.6409). Figure 15(b) shows the signal $x(t)$ waveform diagrams, which still shows the neuromorphic firing behavior. Here, we see that for the limit cycle, the number of the spiking is the same, while for the chaotic attractor, the number of the spiking oscillates randomly. The phase trajectories in the $x - w$ plane are shown in Figure 15(c). The basin of attraction is depicted in Figure 15(d). Moreover, the region of chaotic oscillation is expressed by cyan, the blue region exhibits the dynamics of periodic. Various fractal structures are explored by utilizing the basin of attraction.

## 5. Circuit Implementation Based on STM32

In this section, system (1) is verified by digital circuit experiment based on MCU development tool. This experiment takes STM32F103 development board and TLV5618 of 12 bit DAC module as the core to discretize the continuous chaotic system, and the following discrete system equation (11) can be obtained. On the oscilloscope of the SDS1102X, the chaotic phase trajectories are shown in Figure 16.

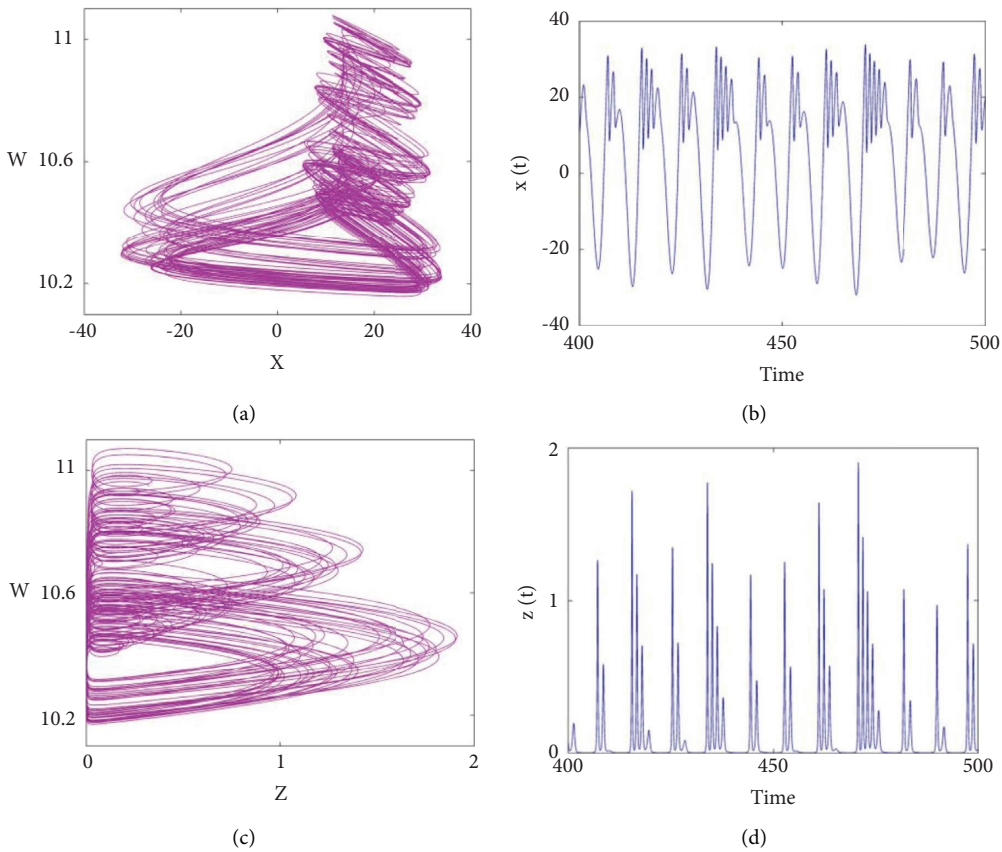


Figure 12: Chaotic bursting with $a = 0.4$, $b = 0.05$, $c = 20$, and IC = (−9, 0, 0, −1). (a) $x - w$. (b) Signals $x$ $(t)$. (c) $z - w$. (d) Signals $z$ $(t)$.

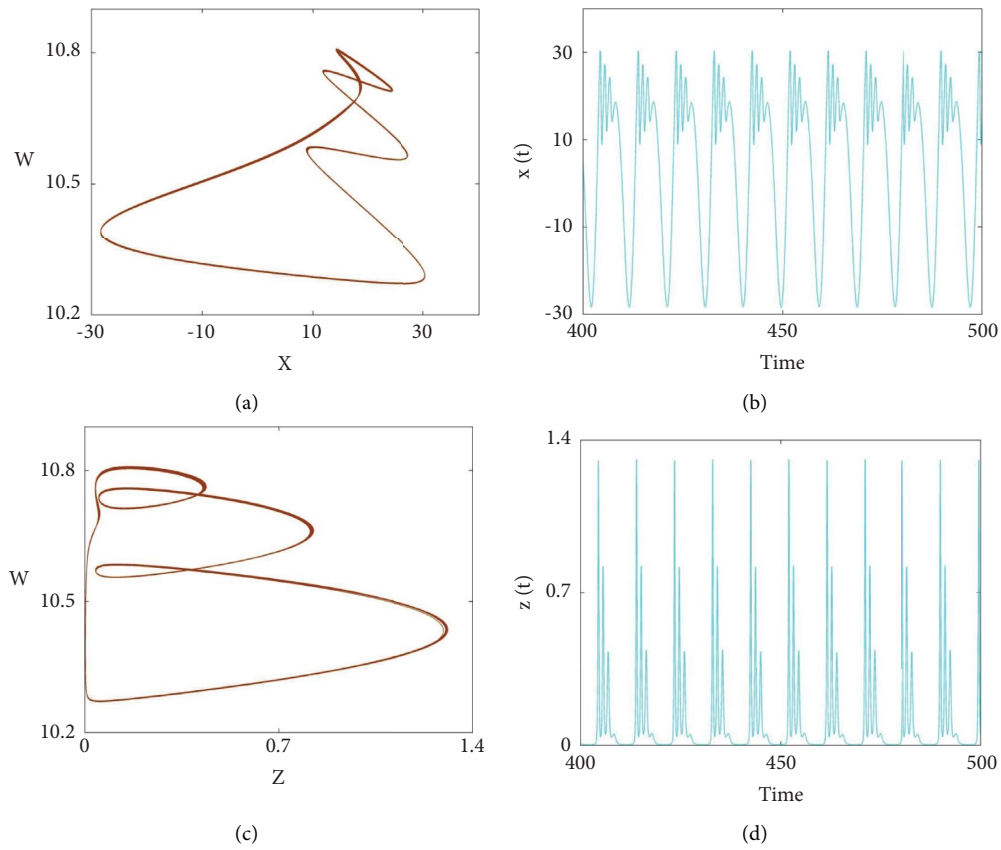


Figure 13: Period bursting firing with $a = 0.4$, $b = 0.1$, $c = 20$, and IC = (−9, 0, 0, −1). (a) $x - w$. (b) Signals $x$ $(t)$. (c) $z - w$. (d) Signals $z$ $(t)$.

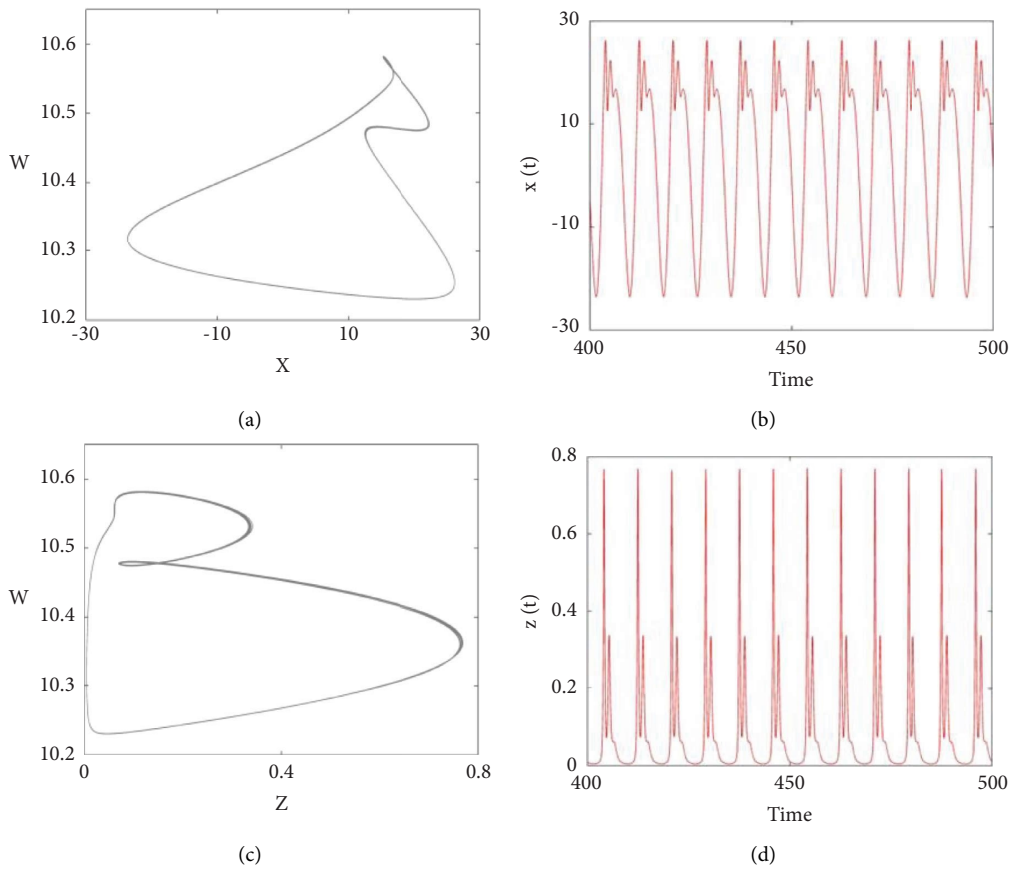


Figure 14: Period bursting firing with $a = 0.4$, $b = 0.2$, $c = 20$, and IC = (−9, 0, 0, −1). (a) $x - w$. (b) Signals $x(t)$. (c) $z - w$. (d) Signals $z(t)$.

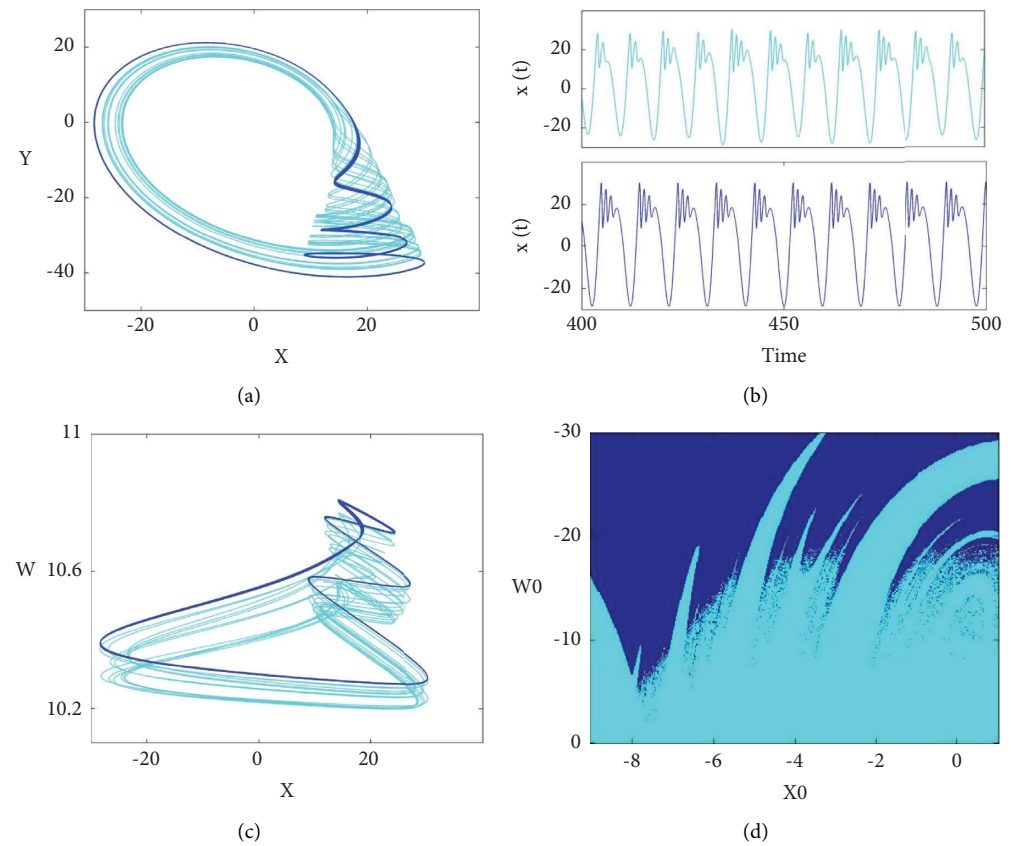


Figure 15: Coexisting attractors in system (1) with $a = 0.4$, $b = 0.1$, and $c = 20$, under different initial conditions. (a) $x - y$. (b) Signals $x(t)$. (c) $x - w$. (d) Basin of attraction: $x_0 - w_0$ ($y_0 = 0$, $z_0 = 0$). (IC = (−9, 0, 0, −10) is cyan, IC = (−9, 0, 0, −20) is blue.)

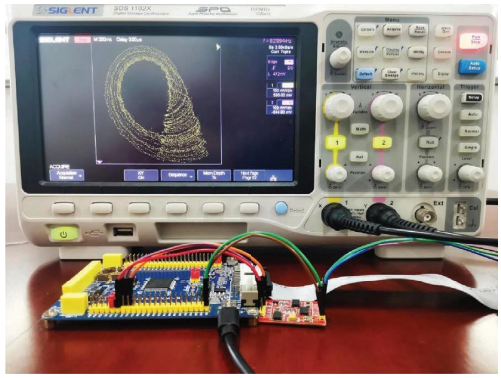

Figure 16: Hardware implementation based on STM32 for system (1).

(a) (b)

Figure 17: Chaotic attractors of system (1). (a) $x-y$. (b) $x-z$.

(a) (b)

Figure 18: Different types of firing patterns of system (1). (a) Chaotic attractor for $b=0.05$. (b) Period-2 attractor for $b=0.2$.

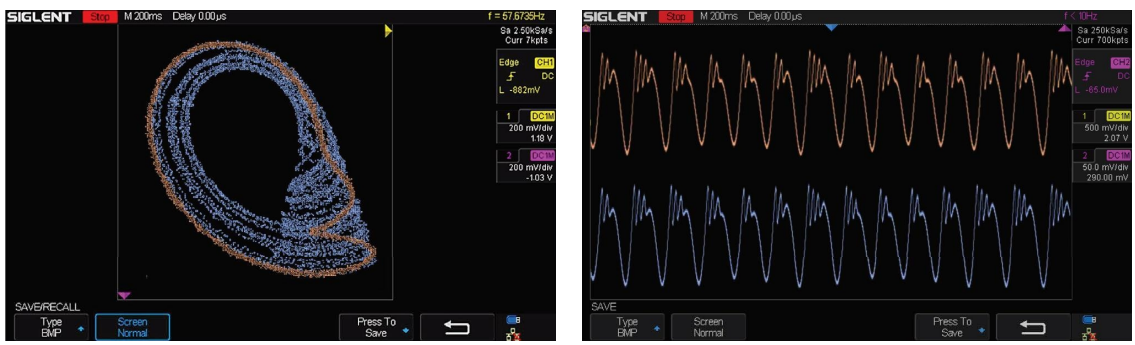

(a) (b)

Figure 19: Coexisting attractors in system (1) with $a=0.4$, $b=0.1$, and $c=20$, under different initial conditions. (a) $x-y$. (b) Signals $x(t)$. (IC = (−9, 0, 0, −10) is light blue, IC = (−9, 0, 0, −20) is brown.)

$$\begin{cases} x(n+1) = x(n) + \left(-y(n) - z(n)w^2(n)\right)\Delta T, \\ y(n+1) = y(n) + (x(n) + 0.4y(n))\Delta T, \\ z(n+1) = z(n) + (0.05 + z(n)(x(n) - 20))\Delta T, \\ w(n+1) = w(n) + (0.2(30 - w(n) + |w(n) - 20| - |w(n) - 40|) + z(n))\Delta T. \end{cases} \tag{11}$$

The $\Delta T$ in the equation (11) is the time interval for calculating the discrete points, and the accuracy of the experimental data was chosen to be $\Delta T = 0.05$ for this experiment in order to be guaranteed. The main control chip is the STM32F103VET, a 32 bit machine with a main frequency of up to 72 MHz. The TLC5618 is used to output two separate signals via two 12 bit DAC modules. By setting initial conditions and parameters, the phase trajectories of system (1) can be observed, as shown in Figure 17. The neuronal firing behavior that appears in the output signal $x(t)$ and $z(t)$ waveforms for choosing different parameters $b$ is shown in Figure 18. The coexisting attractors of the system that appears are shown in Figure 19, where IC = (−9, 0, 0, −10) is light blue, IC = (−9, 0, 0, −20) is brown. Obviously, the results will validate the numerical simulation results.

## 6. Conclusion

When a locally active memristor is applied in the Rössler system, neuron-like chaotic firing is observed. Multiple patterns of neuronal firing are captured including coexisting periodic and chaotic oscillations and some other separate ones. By changing the initial conditions of the system, the system gives the coexisting behaviours of the periodic and chaotic states. Because of the memory effect of the memristor, two parameters in the system equation show local amplitude control. One of the parameters rescales simultaneous regulation of the amplitude and frequency of the firing, while the other parameter enables amplitude control. Finally, the neuronal firing and coexisting attractors in the system are verified based on the STM32 experiment.

## Data Availability

The data that support the findings of this study are available from the corresponding author upon reasonable request.

## Conflicts of Interest

The authors declare that they have no conflicts of interest.

## Acknowledgments

This work was supported financially by the National Natural Science Foundation of China (Grant No. 61871230), and a project funded by the Priority Academic Program Development of Jiangsu Higher Education Institutions.

## References

[1] L. O. Chua, "Memristor-the missing circuit element," *IEEE Transactions on Circuit Theory*, vol. 18, no. 5, pp. 507–519, 1971.

[2] L. O. Chua and S. M. Kang, "Memristive devices and systems," *Proceedings of the IEEE*, vol. 64, no. 2, pp. 209–223, 1976.

[3] C. Li, J. C. Sprott, W. Thio, and H. Zhu, "A new piecewise linear hyperchaotic circuit," *IEEE Transactions on Circuits and Systems II: Express Briefs*, vol. 61, no. 12, pp. 977–981, 2014.

[4] S. P. Adhikari, M. P. Sah, H. Kim, and L. O. Chua, "Three fingerprints of memristor," *IEEE Transactions on Circuits and Systems I: Regular Papers*, vol. 60, no. 11, pp. 3008–3021, 2013.

[5] J. M. Tour and T. He, "Electronics: the fourth element," *Nature*, vol. 453, no. 7191, pp. 42-43, 2008.

[6] M. Di Ventra, Y. V. Pershin, and L. O. Chua, "Circuit elements with memory: memristors, memcapacitors, and meminductors," *Proceedings of the IEEE*, vol. 97, no. 10, pp. 1717–1724, 2009.

[7] X. Zhang, C. Li, E. Dong, Y. Zhao, and Z. Liu, "A conservative memristive system with amplitude control and offset boosting," *International Journal of Bifurcation and Chaos*, vol. 32, no. 04, Article ID 2250057, 2022.

[8] D. B. Strukov, G. S. Snider, D. R. Stewart, and R. S. Williams, "The missing memristor found," *Nature*, vol. 453, no. 7191, pp. 80–83, 2008.

[9] C. Li, W. Hu, J. C. Sprott, and X. Wang, "Multistability in symmetric chaotic systems," *The European Physical Journal - Special Topics*, vol. 224, no. 8, pp. 1493–1506, 2015.

[10] Y. Li, C. Li, S. Zhang, G. Chen, and Z. Zeng, "A self-reproduction hyperchaotic map with compound lattice dynamics," *IEEE Transactions on Industrial Electronics*, vol. 69, no. 10, pp. 10564–10572, 2022.

[11] C. Li, J. C. Sprott, X. Zhang, L. Chai, and Z. Liu, "Constructing conditional symmetry in symmetric chaotic systems," *Chaos, Solitons & Fractals*, vol. 155, Article ID 111723, 2022.

[12] H. Lin, C. Wang, Q. Hong, and Y. Sun, "A multi-stable memristor and its application in a neural network," *IEEE Transactions on Circuits and Systems II: Express Briefs*, vol. 67, no. 12, pp. 3472–3476, 2020.

[13] G. D. Leutcho, J. Kengne, L. Kamdjeu Kengne, A. Akgul, V. T. Pham, and S. Jafari, "A novel chaotic hyperjerk circuit with bubbles of bifurcation: mixed-mode bursting oscillations, multistability, and circuit realization," *Physica Scripta*, vol. 95, no. 7, Article ID 075216, 2020.

[14] A. Akgul, I. Moroz, I. Pehlivan, and S. Vaidyanathan, "A new four-scroll chaotic attractor and its engineering applications," *Optik*, vol. 127, no. 13, pp. 5491–5499, 2016.

[15] F. Min, W. Zhang, Z. Ji, and L. Zhang, "Switching dynamics of a non-autonomous FitzHugh-Nagumo circuit with piecewise-linear flux-controlled memristor," *Chaos, Solitons & Fractals*, vol. 152, Article ID 111369, 2021.

[16] Q. Lai, Z. Wan, H. Zhang, and G. Chen, "Design and analysis of multiscroll memristive hopfield neural network with adjustable memductance and application to image encryption,"

*IEEE Transactions on Neural Networks and Learning Systems*, pp. 1–14, 2022.

[17] J. Ma, F. Wu, W. Jin, P. Zhou, and T. Hayat, "Calculation of Hamilton energy and control of dynamical systems with different types of attractors," *Chaos: An Interdisciplinary Journal of Nonlinear Science*, vol. 27, no. 5, Article ID 053108, 2017.

[18] Q. Lai, L. Yang, and Y. Liu, "Design and realization of discrete memristive hyperchaotic map with application in image encryption," *Chaos, Solitons & Fractals*, vol. 165, Article ID 112781, 2022.

[19] X. Gao, J. Mou, L. Xiong, Y. Sha, H. Yan, and Y. Cao, "A fast and efficient multiple images encryption based on single-channel encryption and chaotic system," *Nonlinear Dynamics*, vol. 108, no. 1, pp. 613–636, 2022.

[20] Y. Li, C. Li, Y. Zhao, and S. Liu, "Memristor-type chaotic mapping," *Chaos: An Interdisciplinary Journal of Nonlinear Science*, vol. 32, no. 2, Article ID 021104, 2022.

[21] Q. Lai, C. Lai, H. Zhang, and C. Li, "Hidden coexisting hyperchaos of new memristive neuron model and its application in image encryption," *Chaos, Solitons & Fractals*, vol. 158, Article ID 112017, 2022.

[22] Y. Liang, G. Wang, G. Chen, Y. Dong, D. Yu, and H. H. C. Iu, "S-type locally active memristor-based periodic and chaotic oscillators," *IEEE Transactions on Circuits and Systems I: Regular Papers*, vol. 67, no. 12, pp. 5139–5152, 2020.

[23] N. Wang, G. Zhang, and H. Bao, "Bursting oscillations and coexisting attractors in a simple memristor-capacitor-based chaotic circuit," *Nonlinear Dynamics*, vol. 97, no. 2, pp. 1477–1494, 2019.

[24] J. Ying, Y. Liang, G. Wang, H. H. C. Iu, J. Zhang, and P. Jin, "Locally active memristor based oscillators: the dynamic route from period to chaos and hyperchaos," *Chaos*, vol. 31, no. 6, Article ID 063114, 2021.

[25] L. O. Chua, "Everything you wish to know about memristors but are afraid to ask," *Radioengineering*, vol. 24, no. 2, pp. 319–368, 2015.

[26] Z. Liang, K. Sun, and S. He, "Design and dynamics of the multicavity hyperchaotic map based on offset boosting," *The European Physical Journal Plus*, vol. 137, no. 1, p. 51, 2022.

[27] X. Zhang, C. Li, Y. Chen, H. H. Iu, and T. Lei, "A memristive chaotic oscillator with controllable amplitude and frequency," *Chaos, Solitons & Fractals*, vol. 139, Article ID 110000, 2020.

[28] Y. Jiang, C. Li, C. Zhang, Y. Zhao, and H. Zang, "A double-memristor hyperchaotic oscillator with complete amplitude control," *IEEE Transactions on Circuits and Systems I: Regular Papers*, vol. 68, no. 12, pp. 4935–4944, 2021.

[29] P. Jin, G. Wang, Y. Liang, H. H. C. Iu, and L. O. Chua, "Neuromorphic dynamics of Chua corsage memristor," *IEEE Transactions on Circuits and Systems I: Regular Papers*, vol. 68, no. 11, pp. 4419–4432, 2021.

[30] H. Lin, C. Wang, Y. Sun, and W. Yao, "Firing multistability in a locally active memristive neuron model," *Nonlinear Dynamics*, vol. 100, no. 4, pp. 3667–3683, 2020.

[31] D. Ding, L. Jiang, Y. Hu et al., "Hidden coexisting firings in fractional-order hyperchaotic memristor-coupled HR neural network with two heterogeneous neurons and its applications," *Chaos: An Interdisciplinary Journal of Nonlinear Science*, vol. 31, no. 8, Article ID 083107, 2021.

[32] Y. Tan and C. Wang, "A simple locally active memristor and its application in HR neurons," *Chaos: An Interdisciplinary Journal of Nonlinear Science*, vol. 30, no. 5, Article ID 053118, 2020.

[33] S. Zhang, J. Zheng, X. Wang, Z. Zeng, and S. He, "Initial offset boosting coexisting attractors in memristive multi-double-scroll Hopfield neural network," *Nonlinear Dynamics*, vol. 102, no. 4, pp. 2821–2841, 2020.

[34] J. Ma, F. Wu, G. Ren, and J. Tang, "A class of initials-dependent dynamical systems," *Applied Mathematics and Computation*, vol. 298, pp. 65–76, 2017.

[35] O. E. Rössler, "An equation for continuous chaos," *Physics Letters A*, vol. 57, no. 5, pp. 397-398, 1976.

[36] Q. Xu, X. Tan, D. Zhu, H. Bao, Y. Hu, and B. Bao, "Bifurcations to bursting and spiking in the Chay neuron and their validation in a digital circuit," *Chaos, Solitons & Fractals*, vol. 141, Article ID 110353, 2020.

[37] H. Bao, A. Hu, W. Liu, and B. Bao, "Hidden bursting firings and bifurcation mechanisms in memristive neuron model with threshold electromagnetic induction," *IEEE Transactions on Neural Networks and Learning Systems*, vol. 31, no. 2, pp. 502–511, 2020.

[38] H. Lin, C. Wang, C. Chen et al., "Neural bursting and synchronization emulated by neural networks and circuits," *IEEE Transactions on Circuits and Systems I: Regular Papers*, vol. 68, no. 8, pp. 3397–3410, 2021.